Zinc-blende group III-V/group IV epitaxy: Importance of the miscut

Charles Cornet, Simon Charbonnier, Ida Lucci, Lipin Chen, Antoine Létoublon, Angela Alvarez, Karine Tavernier, Tony Rohel, Rozenn Bernard, Jean-Baptiste Rodriguez, et al.

▶ **To cite this version:**

Charles Cornet, Simon Charbonnier, Ida Lucci, Lipin Chen, Antoine Létoublon, et al.. Zinc-blende group III-V/group IV epitaxy: Importance of the miscut. Physical Review Materials, 2020, 4 (5), pp.053401. 10.1103/PhysRevMaterials.4.053401 . hal-02878985

HAL Id: hal-02878985
https://hal.science/hal-02878985v1

Submitted on 2 Jul 2020

HAL is a multi-disciplinary open access archive for the deposit and dissemination of scientific research documents, whether they are published or not. The documents may come from teaching and research institutions in France or abroad, or from public or private research centers.

L'archive ouverte pluridisciplinaire **HAL**, est destinée au dépôt et à la diffusion de documents scientifiques de niveau recherche, publiés ou non, émanant des établissements d'enseignement et de recherche français ou étrangers, des laboratoires publics ou privés.

Zinc-Blende group III-V/group IV epitaxy: importance of the miscut

C. Cornet[1,*], S. Charbonnier[2], I. Lucci[1], L. Chen[1], A. Létoublon[1], A. Alvarez[1], K. Tavernier[1], T. Rohel[1], R. Bernard[1], J.-B. Rodriguez[4], L. Cerutti[4], E. Tournié[4], Y. Léger[1], M. Bahri[5], G. Patriarche[5], L. Largeau[5], A. Ponchet[3], P. Turban[2] and N. Bertru[1]

[1]*Univ Rennes, INSA Rennes, CNRS, Institut FOTON – UMR 6082, F-35000 Rennes, France*
[2]*Univ Rennes, CNRS, IPR (Institut de Physique de Rennes) - UMR 6251, F-35000 Rennes, France*
[3]*CEMES-CNRS, Université de Toulouse, UPS, 29 rue Jeanne Marvig, BP 94347 Toulouse Cedex 04, France*
[4]*IES, Univ. Montpellier, CNRS, Montpellier, France*
[5]*Université Paris-Saclay, CNRS, Centre de Nanosciences et de Nanotechnologies, 91120, Palaiseau, France*

Here, we clarify the central role of the miscut during group III-V/ group IV crystal growth. We show that the miscut impacts the initial antiphase domain distribution, with two distinct nucleation-driven (miscut typically >1°) and terraces-driven (miscut typically <0.1°) regimes. It is then inferred how the antiphase domain distribution mean phase and mean lateral length are affected by the miscut. An experimental confirmation is given through the comparison of antiphase domain distributions in GaP and GaSb/AlSb samples grown on nominal and vicinal Si substrates. The antiphase domain burying step of GaP/Si samples is then observed at the atomic scale by scanning tunneling microscopy. The steps arising from the miscut allow growth rate imbalance between the two phases of the crystal and the growth conditions can deeply modify the imbalance coefficient, as illustrated with GaAs/Si. We finally explain how a monodomain III-V semiconductor configuration can be achieved even on low miscut substrates.

I. INTRODUCTION

The monolithic integration of both Zinc-Blende and Wurtzite III-V semi-conductors respectively on (001) and (111) group-IV substrates (such as Si or Ge), is nowadays one of the most promising approach for the development of integrated photonic devices, or efficient energy production and storage applications [1–3]. More specifically, (001) substrates are generally preferred over (111) ones, as they are expected to ease the post-growth processing of group III-V/ group IV devices [1]. On the other hand, crystal defects generated in III-V epilayers grown on group IV substrates may be numerous and detrimental for devices operation. Especially, antiphase domains (APDs) which are related to the polar on non-polar epitaxy (i.e. to the two different ways for the III-V atoms to be allocated at the group IV substrate surface) strongly impact the structural, and electronic properties of grown III-V semiconductors. The easiest solution to avoid or mitigate the formation and propagation of antiphase boundaries (APBs) through the device itself is to grow the III-V materials on misoriented group IV (001) substrates. But the post-growth processing of such misoriented (vicinal) III-V/IV wafers remains tricky [1], especially when the miscut angle reaches 1° or more. Recently, many research groups tried to reduce or even suppress the miscut of the used group-IV wafer. [4,5] But a clear view on the relationship between miscut, APBs generation, and APBs propagation is still missing.

Indeed, the use of a vicinal substrate is often motivated by the ability to promote the double step formation at the group IV surface [6], avoiding the monoatomic layer translation of the III-V crystal which may appear due to the presence of single steps at the substrate surface, theoretically generating an APB. With this picture in mind, K. Volz *et al.* explained their results about epitaxial GaP/Si by considering a 2D III-V growth mode on the substrate [7] (Note that the difference between a 2D growth mode and a flat 3D one is difficult to make experimentally).

On the other hand, the recent work by I. Lucci *et al.* proposes an alternative model [8] based on Density Functional Theory calculation and the extensive characterization of a variety of GaP/Si, AlSb/Si and AlN/Si samples. This model can be summarized as follow: (i) There is only a partial wetting between III-V semiconductors and Si, thus leading to the formation of pure 3D Volmer-Weber growth mode, as experimentally confirmed by some other studies [9,10]. AlSb/Si islands have even been found to be at their equilibrium shape. [9] This model can be generalized to the epitaxy of III-V on Ge, based on the surface energy involved and the experimental results found in the literature [11]. (ii) APBs are generated during the coalescence of 3D islands having different phases, as also suggested in pioneering works on III-V/Ge [11]. The size of individual monodomain islands can be much larger than the distance between steps (the terrace width) [8], which suggests that the step itself cannot be the main cause for the APDs generation. (iii) Elastic energy does not have a significant impact on the island morphology at the coalescence growth step (and therefore does not impact the APD distribution), as most of the islands are already

Accepted manuscript

plastically relaxed (even for GaAs/Si [12]) at this stage (or unstrained in the particular case of the quasi-lattice-matched GaP/Si system). (iv) The epitaxial relationship is defined locally at the nucleation site which further governs the phase distribution.

Meanwhile, extensive works were performed about the dislocation-free GaP/Si model case. A clear correlation between the Si local surface dimer orientation and the subsequent epitaxial III-V phase was established (See for instance ref. [13] or [14] and references therein). This led the authors to support the idea of a step-induced generation of APBs. Although these observations may seem in contradiction with the model involving the nucleation of monodomain islands described previously, the connection will be established later on in this work. Finally, many groups tried to favor the so-called APB annihilation by playing with the III-V growth parameters. It was noticed that the V/III ratio and growth temperature play an important role in this process [15,16], suggesting a significant contribution of kinetic effects at this stage.

In this work, we aim to clarify the impact of the miscut on the generation of antiphase domains during the heteroepitaxy of group III-V semiconductors on group IV substrates. We first investigate the influence of the miscut on the initial APD distribution, in the low and large miscut regimes. It is then proposed that the growth rate imbalance between the two III-V phases is the main driving force for the APD burying. The possibility to leverage this mechanism in the case of very low miscut substrates is finally discussed.

II. THE INITIAL PHASE DISTRIBUTION

Before any other consideration, the link between the initial phase distribution in the III-V layer (i.e. the phase distribution after the growth of only a few nanometers) and the group IV substrate surface properties should be made. In this section we first review the results of the literature about phase distributions in III-V/IV materials systems, and show how it connects to the substrate properties, and especially to the miscut. We then infer the important physical parameters that characterize the initial phase distribution, and their link with the group IV substrate surface properties.

A. The critical miscut

In order to clarify the impact of the miscut on the initial distribution of III-V islands phase we first analyze the results of the literature. In the following, all the works reported here use a miscut along the [110] direction. For low miscut Si substrates (typically <1°), Beyer et al. [14] have demonstrated that the APD distribution in the GaP crystal reproduces well the distribution of steps at the Si surface. For large miscut (typically >1°), on the contrary, many studies report on APD sizes significantly larger than the average terrace width. For the MOCVD growth of GaP on 2°-off Si (corresponding to an average terrace width of 3.89 nm), 9 to 26 nm-large APDs were observed [17]. For the MBE growth of GaP on 4°-off Si (average terrace width of 1.94 nm), a complete analysis of the APD distribution led to the conclusion that the APD lateral width typically falls in the 10 to 58 nm range [16]. Finally, APDs with an average width of 12 nm were found for the MBE growth of GaP on 6°-off Si substrates (average terrace width of 1.29 nm) [8,18,19]. Additionally, on Si-6°-off substrates again, 10-50 nm large islands were determined for the MBE growth of AlSb/GaSb on Si [9]. From all these results, it therefore appears that the APDs morphology are somewhat related to the steps distribution at the group-IV surface only when the III-V growth is performed on low miscut substrates. It is markedly not the case when the III-V growth is performed on large miscut group IV substrates, because the average APD width is systematically larger than the terrace width.

Also, only a partial wetting of the group-IV surface by the III-V is theoretically expected and experimentally observed [8,9]. Therefore, it is reasonable to postulate that the III-V growth on group IV substrate starts with the formation of monodomain III-V 3D islands, whose phase is defined directly by the surface dimer orientation at the nucleation site. In the case of low miscut group IV substrates (see Fig. 1(a)), terraces are large, and several III-V islands with the same phase can therefore grow on the same terrace. After coalescence of these islands, the APD distribution thus mimics the terrace distribution: the APBs will approximately follow the monoatomic step edges initially existing at the group IV substrate surface. But it is only an approximation, as before coalescence individual islands may grow over a Si monoatomic step while staying monodomain, as schematically represented in Fig. 1(a). Thus, for low miscut substrates, the lateral size of APDs is expected to be directly related to the average lateral size of the substrate surface terraces. The APD distribution is therefore "terraces-driven".

By contrast, large miscut group-IV substrates result in narrow terraces. The typical size of the monodomain III-V islands is in that case larger than the width of terraces (see Fig. 1(b)). This leads to a "nucleation-driven" APD distribution, where the lateral size of the APDs after coalescence is mainly related to the distance between two neighboring islands of opposite phases.

The frontier between the terraces-driven and the nucleation-driven APD generation regimes corresponds to the situation where the average width of the terraces at the group IV substrate surface equals the average distance between two neighboring islands of opposite phases along the miscut direction. The corresponding miscut angle is named hereafter the "critical miscut". The value of the critical miscut depends on the initial density of nucleation sites and therefore directly depends on the nature of the III-V material, as well as on the growth conditions at the nucleation stage.

Figure 1(c) represents the evolution of the average terrace width as a function of the miscut angle, for a silicon surface

Accepted manuscript

composed of monoatomic steps. We note here that this trend is also valid for a Ge surface. In fact, terrace widths for a given miscut angle are only marginally different for Ge compared to Si at the scale of the process described here. The average distance between two neighboring islands along the miscut direction d_{1D} can be calculated from the island density d measured experimentally by considering a Poisson distribution of the III-V islands positions at the group-IV surface [20] :

$$d_{1D} = \frac{1}{\pi\sqrt{d}} \qquad (1)$$

The average distance between two neighboring islands along the miscut direction was extracted for different III-V/IV systems studied in the literature using equation (1): GaSb/Si [21], AlSb/Si [21], GaP/Si [8], InP/Si [22], GaAs/Si [23,24] and GaAs/Ge [11]. In these works, islands are observed well after the nucleation step. Therefore, the island density is not expected to change during the growth, and would remain the same for thicker layers at the coalescence step. The values extracted here can thus be used to derive the critical miscut corresponding to the growth conditions reported in these papers. To this end, the average distance between two neighboring islands calculated for each of the reference above are plotted with colored dots on the "Terrace-width *vs* Miscut angle" curve in Fig. 1(c).

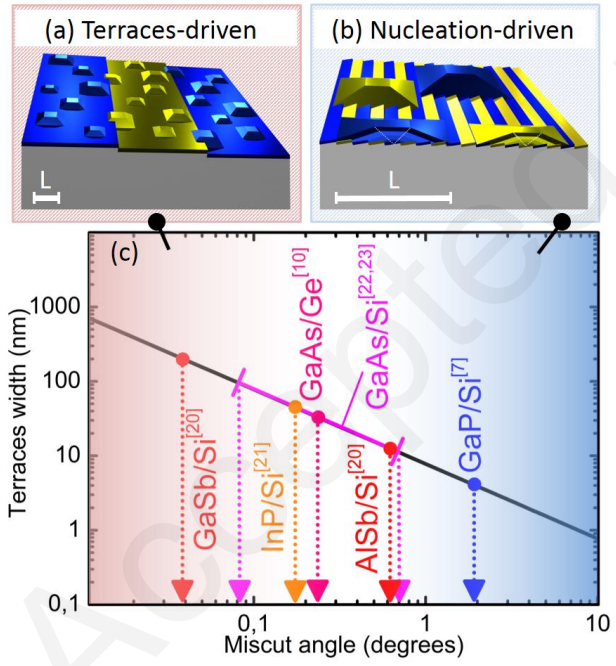

FIG. 1: Sketch of (a) the terraces-driven phase distribution in III-V islands grown on low miscut group IV substrates, and of (b) the nucleation-driven phase distribution in III-V islands grown on large miscut group IV substrates. Blue and yellow colors are used to indicate the different surface dimer orientations and phases of both group IV terraces and III-V islands. L indicates the mean size of III-V islands. (c) Average length of terraces along the [110] or [1-10] directions as a function of the miscut angle for Si or Ge surfaces composed of monoatomic steps. Colored dots correspond to the 1D average distance between islands reported for different III-V/group IV systems, from refs. [8,11,21–24]. The vertical dashed arrows indicate the corresponding critical miscuts.

Dashed arrows in Fig. 1(c) represent the critical miscuts between the two APD generation regimes for each material system for the corresponding growth conditions. Red and blue miscut ranges are highlighted in Fig. 1(c) and are regions where terraces-driven and nucleation-driven APD distribution are respectively likely to occur. Of course, in addition to the growth conditions used during the nucleation, number of parameters could have an impact on the critical miscut, including the actual number of steps at the surface and the growth technique chosen (e. g. Molecular Beam Epitaxy (MBE) or Metal-Organic Chemical Vapor Deposition (MOCVD)). Nevertheless, except in some extreme epitaxial conditions [25], most of the previous works report island surface densities in the $[10^9\text{-}10^{11}]$ cm^{-2} range, which allow concluding that the critical miscut is in the [0.1-1] ° range for common group III-V/group IV heterogeneous associations.

B. The antiphase domain initial distribution

Overall, the initial APD distribution (very near the III-V/group IV interface) can be fully characterized by two parameters. First, the III-V crystal mean phase can be characterized by a single number ranging from -1 to +1 [18,26]. Here, considering APBs propagating vertically, a mean phase of 0 means an equal number of atoms in the main phase and antiphase domains. The island nucleation being a stochastic process, the mean phase is directly related to the area ratio between the two different group IV substrate terraces local surface dimer orientations. Note that for a given III-V crystal mean phase, many different monoatomic or biatomic group IV steps possible configurations may be considered. Inversely, a given average density of monoatomic steps at the substrate surface is not enough to predict the mean phase of the III-V crystal, as the in-plane distribution of monoatomic steps can significantly change the mean phase of the III-V crystal. Therefore, the achievement of statistically-dominant biatomic steps distribution at the surface certainly helps to promote a near to single phase domain configuration (i.e. a mean phase of +1 or -1) in III-V layers [27].

The second important parameter is the mean lateral extent of APDs, which is related either to the terrace width below the critical miscut, or to the nucleation islands density above the critical miscut. Here, it should be mentioned that the concept of critical miscut was introduced by considering a perfect monoatomic step lattice at the group IV surface. But, depending on the strategy used to prepare the group IV substrate (e.g. chemical preparation or homoepitaxy), the

Accepted manuscript

real step distribution can be quite different from the ideal one. Especially, for low miscut substrates, a fine control of the miscut angle and the miscut direction in addition to a proper homoepitaxial or passivation strategy is needed to reach the perfect terraces-driven APD distribution regime over the whole sample [14].

III. EXPERIMENT

On the basis of the general framework given in sec. I establishing the link between the group IV substrate surface and the initial III-V phase distribution, the evolution of such a phase distribution with the III-V thickness can then be discussed. To this aim, structural properties of thick III-V layers grown on different Si substrates with low and large miscuts were studied and compared.

In Fig. 2, a comparison between similarly thick III-V layers grown on low and large miscut group IV substrates is shown. Growth and microscopy details are given in the supplemental materials [20]. First, cross-sectional Transmission Electron Microscopy (TEM) images of two comparable samples mainly composed of GaSb (with a thin AlSb nucleation layer) grown on freshly prepared [28] Si 0.3°-off toward the [110] direction (Fig. 2(a)) and 6°-off toward the [110] direction (Fig. 2(b)) are shown. In these images, bright and dark areas correspond to the main phase or antiphase domains contrasts, although the presence of other defects may contribute as well. At first sight, it can be seen that APDs are overall larger and taller for the low miscut case than for the large miscut case.

More specifically, the two images show two distinct features: (i) the presence of very small APDs very near the interface, with a typical width smaller than 20nm, and a height smaller than 50 nm, which corresponds to the size of the individual islands formed initially [8]. These small APDs are numerous for large miscut samples, although some small APDs can also be seen in the low miscut case. (ii) Some large APDs, with a width typically larger or much larger than 20 nm, and a vertical extent larger than 50-nm which correspond to the APD distribution after the burying of the previously discussed small APDs. This apparent bimodal distribution may be related to the adatom diffusion length needed for APD burying, which will be discussed later on in this paper.

Regarding the initial APD distribution, *i.e.* near the III-V/Si interface, it can be seen that while the GaSb growth on 6°-off Si leads to very small dark and bright areas observed all along the interface in the III-V region, the growth on low miscut substrate gives rise to large single-phase areas between two APBs. Indeed, in the low miscut case, following a direction parallel to the III-V/Si interface in close vicinity to the interface, single-phase areas are observed over 40 nm and even beyond, while for the large miscut case, single-phase areas extend at the maximum over 15 nm laterally. This observation is in good agreement with the previously proposed explanation of the impact of the miscut on initial APD distribution.

For samples grown on 6°-off substrate, few large APDs are still visible (see e.g. the one highlighted with dashed line in Fig. 2(b)), but they are on average smaller than the one found in samples grown on (001) substrates (see e.g. the one highlighted with dashed line in Fig. 2(a)). Furthermore, a monodomain GaSb layer is finally reached for the vicinal case, while APBs are propagating until the surface for the nominal one, as shown in the supplemental materials [20].

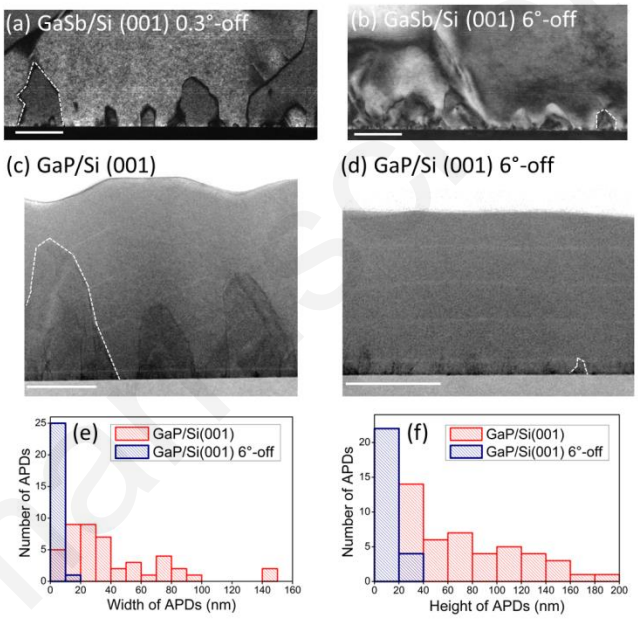

FIG. 2: Cross-sectional Transmission Electron Microscopy images of thick (a) GaSb/Si(001) 0.3°-off, (b) GaSb/Si(001) 6°-off, (c) GaP/Si(001) and (d) GaP/Si(001) 6°-off samples along the [110] direction. For GaSb/Si (a&b), the Si substrate is the black area at the bottom of the images. For GaP/Si (c&d), the Si substrate is the bright grey area at the bottom of the images. The white bar represents 100nm for each TEM image. Dashed lines are guide to the eyes showing typical APBs shape in the sample. Corresponding antiphase domains width (e) and height (f) distributions are quantitatively represented for GaP/Si samples on both nominal and vicinal substrates.

But a meaningful quantitative assessment cannot be given from these pictures, because other defects, such as dislocations [29], introduce a superimposed contrast which complicates the analysis. A more ideal case can be found with the quasi-lattice-matched GaP/Si system. Cross-sectional Transmission Electron Microscopy (TEM) images of two comparable samples (with the same growth conditions) mainly composed of GaP grown on freshly prepared [30] Si (001) (0 +/- 0.5°) substrate (Fig. 2(c)) and 6°-off along the [110] direction (Fig. 2(d)) are shown. It is useful to recall that the exactly oriented nominal group IV (001) substrate is a theoretical case, not achievable by substrate manufacturers. In practical cases, a residual and

often uncontrolled miscut should always being considered [7]. Bright and dark contrasts are again attributed to domains with different phases. A statistical analysis was performed over a cumulated width of 4 µm along the [110] direction (see examples of TEM images in the supplemental materials [20]). Values collected for the APDs width and heights are given in Fig. 2 (e) and (f). APBs emerging at the surface observed for the (001) case are not considered for this analysis. A perfect deconvolution between small APDs and large APDs populations is not achievable, but the images as well as the statistics clearly show that small APDs, near the III-V/Si interface are more numerous and smaller on 6°-off substrates, which tends to confirm the impact of the Si terraces width in the low miscut limit. We also confirm quantitatively that large APDs are much larger on the nominal substrate, and propagate farther in the sample. Finally, Fig. 2(c) also points out that APBs induce roughness and faceting [31] with consequences well after their annihilation. Indeed, it can be seen on the three APBs shown in Fig. 2(c) that the flatness of the free surface is directly related to the distance to the highest point of the buried APD. After a given thickness, the (001) surface is recovered, as shown for the central APD of Fig. 2(c). A thin buffer layer is therefore needed after APBs annihilation to smoothen the surface.

Overall, these images confirm the central role of the miscut on the initial APD distribution, but also point toward the importance of the miscut on the subsequent III-V growth steps.

IV. PHASE DISTRIBUTION EVOLUTION

The experimental observations of sec. III demonstrate that the initial phase distribution discussed in sec. II evolves during the growth and may lead in some cases to mono-domain III-V crystals. In the following, we first investigate how and at which condition the miscut enables burying the antiphase domains. We then introduce, and calculate for GaAs/Si, the growth rate imbalance coefficient, the value of which determines the dominant phase that will develop in the sample and the rate at which it will occur.

A. Antiphase domain burying

The role of the miscut in the so-called APB annihilation process still needs to be clarified. Numbers of situations were reported in the literature ranging from annihilation achieved on large miscut group IV substrates [26] or nominal substrates with a residual miscut (<0.2°) [7], by MBE [16], or by MOCVD [17]. In these references, and in the Fig. 2 TEM images, various APBs profiles are observed, with single or many facets composing the APB. A more precise idea of the mechanisms involved during the "annihilation process" can be obtained by imaging the morphology of the surface precisely at the moment where one domain becomes statistically dominant over the other one. To this aim, a 200-nm thick GaP layer was grown on a Si (001) – 6°-off substrate (see the supplemental materials [20] for growth details). The growth conditions have been chosen such that GaP would become purely monodomain for a thickness of about 300 nm. The sample was then transferred to a Scanning Tunneling Microscope (STM) chamber [20,32] for further surface investigation at the atomic scale. The STM image obtained is shown in Fig. 3(a). The local crystallographic directions of the two different GaP phases can be distinguished at the atomic scale by the surface reconstructions, as shown in Fig. 3(a) inset. Interestingly, the surface is covered by elongated domains either along the [110] direction of the Si substrate, or along its [1-10] direction. Since GaP domains are always elongated along their own [-110] local direction, the two phases are therefore easily distinguishable, even at the microscopic scale.

With this in mind, one can now study in Fig. 3(a) the way one domain dominates the other. Especially, it can be seen that the GaP domains having their [-110] direction parallel to the [110] direction of the Si substrate seem to coalesce through the continuous growth of material over the other phase, leading to the formation of larger single phase domains at the surface. We note here that for given growth conditions, and similar substrates, the dominant phase is consistently the same at the wafer level, as shown in the supplemental materials [20]. Based on this analysis, it is now clear that the annihilation of APBs is simply the result of the antiphase domains burying. This important finding implies that the two different domains have different growth rates despite the fact that they are made of the same material. This is somehow surprising since the two domains have the same (001) surfaces at the growth front, and we propose in the following that the substrate miscut plays at this point an important role.

B. The growth rate imbalance

In this paragraph, we explain how the miscut breaks the symmetry between the two different III-V domains. Fig. 3(b) illustrates the impact of the substrate miscut (along the [110] direction in this example) on the III-V layers grown atop. For the sake of simplicity, a (2x4) surface reconstruction is schematically represented at the top surface of the III-V semiconductor (the atomic reconstruction of the steps is not shown). It clearly appears that for one III-V domain, the miscut is transferred along the [110] direction, while it is transferred to the [-110] direction for the other domain. Consequently, one domain will predominantly form A-steps (when their edges are parallel to the group V dimers, which is the case for the yellow domain in Fig. 3(b)), whereas the other domain will form B-steps (blue domain in Fig. 3(b)) [33]. The incorporation rate on A- and B-steps being different [34,35], the growth rates of domains having different phases is thus also expected to be different. It is important to mention that the situation discussed here only applies to the case of vicinal (001) III-V surfaces. Facets of

higher-index are not considered here, although large stable facets (see for instance the presence of (114) ones for GaP/Si in ref. [31]) may develop (depending on the material system and/or the substrate miscut), especially at the APD edges. The presence of these facets certainly has an impact on the growth rates of each domain, but is not expected to modify the conclusion drawn in the present work

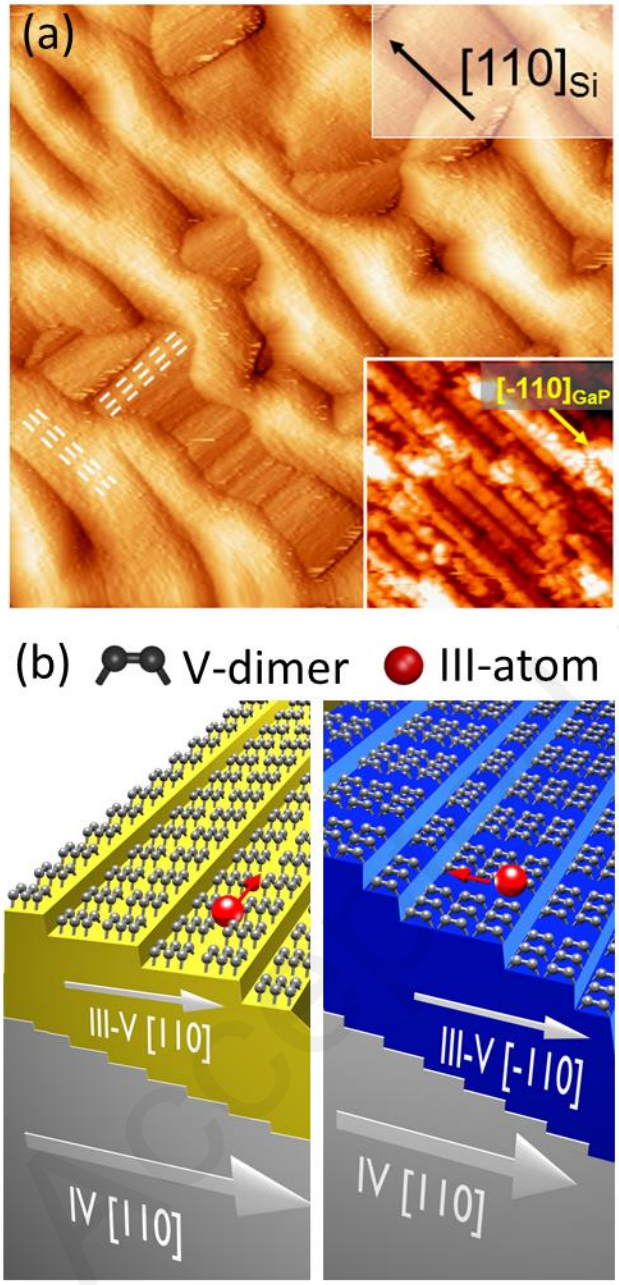

FIG. 3: (a) Plan-view STM image of a 200 nm-thick GaP deposition on Si (001) – 6°-off (400*400 nm2, vertical color scale: 0-13.9nm), during the APB annihilation step. The 19*19 nm^2 inset shows the atomically-resolved morphology of the GaP dominant phase. Dashed lines are guide to the eyes showing local different GaP phases. (b) Illustration of the asymmetry induced by the miscut on the different III-V phases grown on a group IV substrate, enabling different growth rates for the different III-V phases.

In the following, we will call α and β the two different phases of the III-V crystal having respectively more A-steps and B-steps at the surface. The phase α results from the III-V nucleation on a T_α terrace at the Si surface, while the phase β results from the III-V nucleation on a T_β terrace at the Si surface. T_α and T_β are Si terraces with orthogonal surface dimers orientations. The determination of the growth rate imbalance between the α- and the β- phases is therefore of interest, as the early burying of APDs is requested for highly integrated photonics [1] while the propagation of APBs is of interest for some non-linear photonic [26] or water splitting applications [3]. The growth of III-V semiconductors on miscut surfaces may follow two different growth modes, namely step-flow growth or 2D-nucleation ones, or a combination of both [36]. Especially, for given growth conditions, with a very low miscut, the distance between steps at the surface is so large that the growth mostly depends on the diffusion length of adatoms at the surface and 2D-nucleation growth mode arises. For larger miscuts, the incorporation of group-III atoms at the step-edges becomes dominant over all the other contributions, and the step-flow regime is thus favored. This regime corresponds to the situation where the distance between steps is lower than the diffusion length of group-III adatoms, which highly depends on the temperature. [36] The typical values of the diffusion lengths given for group-III adatoms on a III-V planar surface are in the [0.5-1] µm range [15], implying that the miscut at which step-flow growth mode may occur is typically larger than [0.01-0.03]°, depending on the material system and growth conditions. In the present case, a pure 2D nucleation growth mode would result in the same growth rates for the α- and β- phases because the step-edges are only marginally involved in that case. Some fraction of step-flow is therefore required to observe a growth rate difference between α- and β- phases. Therefore, one can conclude that burying of APDs is only possible if the substrate has at least a projected miscut of 0.03° precisely along a given [110] or [1-10] direction. Beyond this value, the respective growth rates of phases α and β only depend on the incorporation rates at steps A and B.

We now introduce the growth rate imbalance coefficient $C_{\alpha/\beta}$ defined as:

$$C_{\alpha/\beta} = \frac{V_{g\alpha}}{V_{g\beta}} = \frac{R^0_A.e^{-\frac{E_A}{k_BT}}}{R^0_B.e^{-\frac{E_B}{k_BT}}} \qquad (1)$$

Where $V_{g\alpha}$ and $V_{g\beta}$ are the crystal growth rates of the phases α and β. $R°_A$, $R°_B$, E_A and E_B, are respectively the amplitudes and energy barriers for direct incorporation at steps A and B, as defined in refs. [34,35]. k_B is the Boltzmann constant, and T the growth temperature.

Therefore, the growth rate imbalance coefficient is a simple ratio between the growth rate of phases α and β, which we can calculate as the ratio of direct step incorporation rate per site for each phase. Therefore, if $C_{\alpha/\beta}$ is lower than unity, the β phase will grow faster than the α one. On the contrary, if $C_{\alpha/\beta}$ is larger than 1, the α phase will become dominant. If $C_{\alpha/\beta}$ equals to one, the growth rates are the same and APBs will propagate to the surface. Interestingly, the development of the α- or β- phases and the rate at which it occurs does not depend on the miscut angle. Indeed, the areal density of steps at the surface of α- and β- phases is the same, whatever the miscut value. APD burying is therefore expected to occur in the same way on low and large miscut group IV substrates, but with different initial phase distributions.

The determination of the growth rate imbalance coefficient requires a solid knowledge of the growth rates or direct step incorporation rates per site for each phase. Experimental determination of the incorporation rates was proposed in the pioneering works of Shitara *et al.* for MBE-grown GaAs, by using reflection high-energy electron diffraction [34,35]. From these data (see supplemental materials for the parameters used [20]), the growth rate imbalance coefficient $C_{\alpha/\beta}$ was calculated as a function of the temperature, for various V/III ratio. The results, shown in Fig. 4, are relevant to the MBE growth of GaAs on Si or Ge substrates (and to some extent to the MOCVD GaAs/Si or GaAs/Ge growth).

Fig. 4 shows that for most growth conditions, the β phase will grow faster than the α one, except at high growth temperature (>600°C) and low V/III ratio (2), where the α phase will be favored. It can also be noticed that the lower the V/III ratio, the more the $C_{\alpha/\beta}$ coefficient becomes sensitive to the growth temperature (slopes of the $C_{\alpha/\beta}(T)$ curves are larger for V/III=2 or 2.5, as compared to the ones for V/III=4.3 or 6.8). As a consequence, in the temperature range shown in Fig. 4, the largest value of $C_{\alpha/\beta}$ is reached for the highest temperature (620°C) and a low V/III ratio (2.0). In that case, $C_{\alpha/\beta}$ is larger than unity and the α phase growth is thus favored. On the other hand, the lowest value of $C_{\alpha/\beta}$ is reached for the lowest growth temperature (540°C) and still a low V/III ratio (2.5), and the β phase will become dominant. This explains the experimental observations given by I. Lucci et al. [31]. In this previous work, thick GaP/Si samples were grown, resulting in a single domain GaP in the central part of the wafer, while at the edges of the 2" wafer, another GaP single domain with opposite phase was observed. The local increasing of the temperature at the edges of the wafer has certainly allowed changing the dominant phase.

It is also interesting to see that, for a given growth temperature (high enough), the V/III ratio may allow to tune the dominant phase at will. This is illustrated in the inset of Fig. 4, where the $C_{\alpha/\beta}$ coefficient was plotted as a function of the V/III ratio for GaAs at a growth temperature of 620°C. By increasing the V/III ratio, the dominant phase changes from α to β. The trends described for GaAs in Fig. 4 are expected to be similar for other III-V semiconductors and thus provide a guide for the growers. A precise determination of the direct step incorporation rates for the different materials systems is however still needed to precisely optimize the heterogeneous group III-V on group IV epitaxy on purpose. The hydrogenation of the surface during MOCVD III-V growth may also significantly impact the step incorporation rates imbalance. We note here that the growth rate imbalance coefficient may also be measured directly for most III-V/IV systems by using direct plan-view imaging on different samples with different thicknesses or cross-sectional imaging on a single sample.

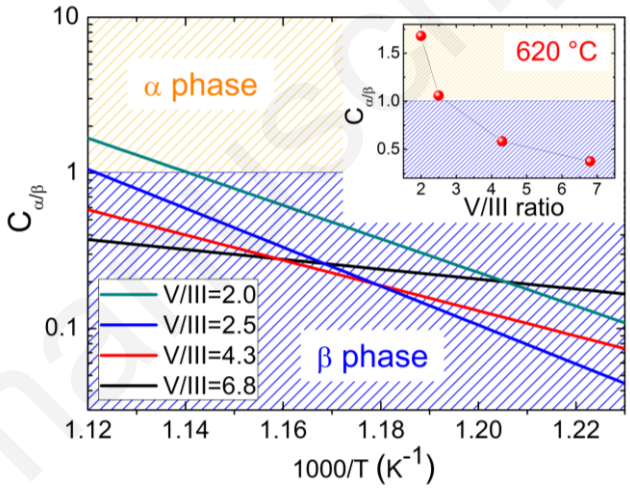

FIG. 4: Growth rate imbalance coefficient $C_{\alpha/\beta}$ as a function of 1000/T for various V/III ratio used in the case of GaAs/group IV epitaxy, determined from ref. [34,35]. The corresponding temperature range is between 540°C and 620°C. The orange area indicates the conditions where the α III-V phase grows faster, while the blue area indicates the conditions where the β III-V phase grows faster. Inset shows the evolution of the imbalance coefficient as a function of the V/III ratio for GaAs grown at 620°C on a group IV substrate.

C. Discussion

The consequences of this antiphase domain burying process description are numerous but we would like to highlight the most important ones. First of all, the mean phase of the initial APD distribution does not impact on the final phase of the layer. Even if the initial T_α/T_β surface ratio is at 80/20, subsequent growth conditions favoring the β phase will lead to a monodomain β-phase crystal after a sufficient thickness. Second, the thickness at which a single domain III-V semiconductor is recovered mainly depends on the initial APD mean lateral extent, and the growth rate imbalance coefficient $C_{\alpha/\beta}$. A large initial APD, as the one observed on nominal substrates in Fig. 2(a) and (c) or in ref. [7], will obviously require a larger deposition thickness to be buried (see fig. 2 e) and f)). In the same way, large

deposition thicknesses will be needed before complete APD burying if growth conditions resulting in $C_{\alpha/\beta}$ close to unity are chosen. Third, the general morphology (and "facets") of APDs is governed by the initial APD distribution as well as by the growth rate imbalance coefficient $C_{\alpha/\beta}$. APBs lying on high-index crystallographic planes certainly reflect a strong growth rate imbalance, *i.e.* $C_{\alpha/\beta}$ much larger or lower than 1. On the contrary, vertical propagation of APBs indicates a $C_{\alpha/\beta}$ coefficient close to 1 or a too low miscut angle, at least locally. This is especially what is currently observed when the growth is performed on standard commercially-available low miscut group IV substrates, where the miscut is not precisely controlled, or when the thermal or chemical substrate preparation does not allow to homogenize the miscut at the wafer scale. We also note that the use of [010] or [100] offcut directions will create the same step density in both directions within one domain, leading therefore to a $C_{\alpha/\beta}$ equals to 1, whatever the growth conditions used in this specific case.

Of course, this general picture does not allow to predict the APB structure at the atomic level, which may be locally impacted by charge compensation effects or temperature-induced kinks, as described by Beyer et al. [37]. Last, from this description it can be understood why burying of APDs can be achieved even on low, but controlled, miscut substrates, if the growth conditions, and especially V/III ratio and growth temperature are carefully chosen to promote growth rate imbalance. Here, we point out that a successful APD burying achieved on a low miscut group-IV substrate requires the precise control of both the miscut angle (larger than 0.03° to keep the step flow growth mode) and the miscut direction, homogeneously at the substrate surface, so that the growth rate imbalance is achieved everywhere in the sample, despite some local miscut direction or angle fluctuations. Thus, the thermal and/or chemical preparation of the group IV wafer prior to the III-V growth, which determines the homogeneity of the miscut and the step distribution at the substrate surface, is undoubtedly the key parameter to achieve a high quality hetero-epitaxial III-V/IV material.

V. CONCLUSIONS

In conclusion, the relationship between the group-IV substrate miscut, and the initial III-V antiphase domain distribution mean phase, and mean lateral size during III-V/group IV epitaxy was clarified. The central role of the miscut in the antiphase domain burying was established. Especially, the miscut was found to induce a growth rate imbalance between the two III-V crystal phases. On this basis it was shown how burying of antiphase domains is possible for low miscut substrates. The detailed description of the group-IV substrate miscut impact on epitaxially grown III-V structural properties opens new prospects for the development of highly integrated photonics or energy production/storage applications.

The authors acknowledge Dr. R. Le Guével and A. de Verneuil for fruitful discussions on the statistical analysis of experimental data for the determination of the critical miscut. Pr. K. Volz and Dr. J.-C. Harmand are also acknowledged for the interesting discussions about III-V/ group IV epitaxial processes. The authors acknowledge RENATECH (French Network of Major Technology Centers) within Nanorennes for technological support. This research was supported by the French National Research Agency ANTIPODE Project (Grant no. 14-CE26-0014-01), ORPHEUS Project (Grant no. ANR-17-CE24-0019-01) and Région Bretagne.

[1] C. Cornet, Y. Léger, and C. Robert, *Integrated Lasers on Silicon* (ISTE-Elsevier, 2016).
[2] H. Cotal, C. Fetzer, J. Boisvert, G. Kinsey, R. King, P. Hebert, H. Yoon, and N. Karam, Energy Environ. Sci. **2**, 174 (2009).
[3] M. Alqahtani, S. Sathasivam, L. Chen, P. Jurczak, R. Piron, C. Levallois, A. Létoublon, Y. Léger, S. Boyer-Richard, N. Bertru, J.-M. Jancu, C. Cornet, J. Wu, and I. P. Parkin, Sustain. Energy Fuels **3**, 1720 (2019).
[4] A. Y. Liu, J. Peters, X. Huang, D. Jung, J. Norman, M. L. Lee, A. C. Gossard, and J. E. Bowers, Opt. Lett. **42**, 338 (2017).
[5] M. R. Calvo, L. M. Bartolomé, M. Bahriz, G. Boissier, L. Cerutti, J.-B. Rodriguez, and E. Tournié, Optica **7**, 263 (2020).
[6] H. Kroemer, J. Cryst. Growth **81**, 193 (1987).
[7] K. Volz, A. Beyer, W. Witte, J. Ohlmann, I. Németh, B. Kunert, and W. Stolz, J. Cryst. Growth **315**, 37 (2011).
[8] I. Lucci, S. Charbonnier, L. Pedesseau, M. Vallet, L. Cerutti, J.-B. Rodriguez, E. Tournié, R. Bernard, A. Létoublon, N. Bertru, A. Le Corre, S. Rennesson, F. Semond, G. Patriarche, L. Largeau, P. Turban, A. Ponchet, and C. Cornet, Phys. Rev. Mater. **2**, 060401(R) (2018).
[9] A. Ponchet, G. Patriarche, J. B. Rodriguez, L. Cerutti, and E. Tournié, Appl. Phys. Lett. **113**, 191601 (2018).
[10] F. Ernst and P. Pirouz, J. Appl. Phys. **64**, 4526 (1988).
[11] P. M. Petroff, J. Vac. Sci. Technol. B **4**, 874 (1986).
[12] R. Hull and A. Fischer-Colbrie, Appl. Phys. Lett. **50**, 851 (1987).
[13] O. Supplie, O. Romanyuk, C. Koppka, M. Steidl, A. Nägelein, A. Paszuk, L. Winterfeld, A. Dobrich, P. Kleinschmidt, E. Runge, and T. Hannappel, Prog. Cryst. Growth Charact. Mater. **64**, 103 (2018).
[14] A. Beyer and K. Volz, Adv. Mater. Interfaces **6**, 1801951 (2019).

Accepted manuscript

[15] J. A. Piedra-Lorenzana, K. Yamane, K. Shiota, J. Fujimoto, S. Tanaka, H. Sekiguchi, H. Okada, and A. Wakahara, J. Cryst. Growth **512**, 37 (2019).
[16] A. C. Lin, M. M. Fejer, and J. S. Harris, J. Cryst. Growth **363**, 258 (2013).
[17] A. Lenz, O. Supplie, E. Lenz, P. Kleinschmidt, and T. Hannappel, J. Appl. Phys. **125**, 045304 (2019).
[18] P. Guillemé, Y. Dumeige, J. Stodolna, M. Vallet, T. Rohel, A. Létoublon, C. Cornet, A. Ponchet, O. Durand, and Y. Léger, Semicond. Sci. Technol. **32**, 065004 (2017).
[19] Y. P. Wang, J. Stodolna, M. Bahri, J. Kuyyalil, T. N. Thanh, S. Almosni, R. Bernard, R. Tremblay, M. D. Silva, A. Létoublon, T. Rohel, K. Tavernier, L. Largeau, G. Patriarche, A. L. Corre, A. Ponchet, C. Magen, C. Cornet, and O. Durand, Appl. Phys. Lett. **107**, 191603 (2015).
[20] See Supplemental Material at [URL will be inserted by publisher] for additional growth details, microscopy analysis and modeling parameters.
[21] K. Akahane, N. Yamamoto, S. Gozu, A. Ueta, and N. Ohtani, J. Cryst. Growth **283**, 297 (2005).
[22] A. Yamamoto, N. Uchida, and M. Yamaguchi, J. Cryst. Growth **96**, 369 (1989).
[23] O. K. Biegelsen, F. A. Ponce, B. S. Krusor, J. C. Tramontana, R. D. Yingling, R. D. Bringans, and D. B. Fenner, MRS Online Proc. Libr. Arch. **116**, (1988).
[24] Y. B. Bolkhovityanov and O. P. Pchelyakov, Phys.-Uspekhi **51**, 437 (2008).
[25] R. Machida, R. Toda, S. Fujikawa, S. Hara, I. Watanabe, and H. I. Fujishiro, Phys. Status Solidi B **253**, 648 (2016).
[26] P. Guillemé, M. Vallet, J. Stodolna, A. Ponchet, C. Cornet, A. Létoublon, P. Féron, O. Durand, Y. Léger, and Y. Dumeige, Opt. Express **24**, 14608 (2016).
[27] M. Martin, D. Caliste, R. Cipro, R. Alcotte, J. Moeyaert, S. David, F. Bassani, T. Cerba, Y. Bogumilowicz, E. Sanchez, Z. Ye, X. Y. Bao, J. B. Pin, T. Baron, and P. Pochet, Appl. Phys. Lett. **109**, 253103 (2016).
[28] K. Madiomanana, M. Bahri, J. B. Rodriguez, L. Largeau, L. Cerutti, O. Mauguin, A. Castellano, G. Patriarche, and E. Tournié, J. Cryst. Growth **413**, 17 (2015).
[29] M. Niehle, J.-B. Rodriguez, L. Cerutti, E. Tournié, and A. Trampert, Acta Mater. **143**, 121 (2018).
[30] T. Quinci, J. Kuyyalil, T. N. Thanh, Y. P. Wang, S. Almosni, A. Létoublon, T. Rohel, K. Tavernier, N. Chevalier, O. Dehaese, N. Boudet, J. F. Bérar, S. Loualiche, J. Even, N. Bertru, A. L. Corre, O. Durand, and C. Cornet, J. Cryst. Growth **380**, 157 (2013).
[31] I. Lucci, S. Charbonnier, M. Vallet, P. Turban, Y. Léger, T. Rohel, N. Bertru, A. Létoublon, J.-B. Rodriguez, L. Cerutti, E. Tournié, A. Ponchet, G. Patriarche, L. Pedesseau, and C. Cornet, Adv. Funct. Mater. 1801585 (2018).
[32] C. Robert, C. Cornet, P. Turban, T. Nguyen Thanh, M. O. Nestoklon, J. Even, J. M. Jancu, M. Perrin, H. Folliot, T. Rohel, S. Tricot, A. Balocchi, D. Lagarde, X. Marie, N. Bertru, O. Durand, and A. Le Corre, Phys. Rev. B **86**, 205316 (2012).
[33] S. B. Zhang and A. Zunger, Mater. Sci. Eng. B **30**, 127 (1995).
[34] T. Shitara, J. Zhang, J. H. Neave, and B. A. Joyce, J. Cryst. Growth **127**, 494 (1993).
[35] T. Shitara, J. Zhang, J. H. Neave, and B. A. Joyce, J. Appl. Phys. **71**, 4299 (1992).
[36] B. A. Joyce, T. Shitara, A. Yoshinaga, D. D. Vvedensky, J. H. Neave, and J. Zhang, Appl. Surf. Sci. **60–61**, 200 (1992).
[37] A. Beyer, B. Haas, K. I. Gries, K. Werner, M. Luysberg, W. Stolz, and K. Volz, Appl. Phys. Lett. **103**, 032107 (2013).

Submitted manuscript